*Proc. Natl. Acad. Sci. USA*
Vol. 93, pp. 27–33, January 1996

# Review

# Functional implications of protein–protein interactions in icosahedral viruses

*John E. Johnson*

*Department of Molecular Biology, The Scripps Research Institute, 10666 North Torrey Pines Road, La Jolla, CA 92037*

**ABSTRACT** **Biological processes often require that a single gene product participate in multiple types of molecular interactions. Viruses with quasiequivalent capsids provide an excellent paradigm for studying such phenomena because identical protein subunits are found in different structural environments. Differences in subunit joints may be controlled by protein segments, duplex or single-stranded RNA, metal ions, or some combination of these. Each of the virus groups examined display a distinctive mechanism for switching interface interactions, illustrating the magnitude of options that are likely to be found in other biological systems. In addition to determining capsid morphology, assembly controls the timing of autocatalytic maturation cleavage of the viral subunits that is required for infectivity in picorna-, noda-, and tetraviruses. The mechanism of assembly-dependent cleavage is conserved in noda- and tetraviruses, although the quaternary structures of the capsids are different as are the molecular switches that control subunit interfaces. The function of the cleavage in picorna-, noda-, and tetraviruses is probably to release polypeptides that participate in membrane translocation of RNA.**

Intermolecular contacts involving different quaternary structures formed from the same gene products are a common feature of biological chemistry. Muscle contraction, for example, requires dramatic alterations in contacts between myosin and actin. Although conformational changes in myosin are driven by ATP hydrolysis, consequent variations at the myosin–actin interface necessitate plastic intermolecular contacts with delicately controlled chemical interactions (1).

Viruses, with quasiequivalent surface lattices, provide an alternative paradigm for the analysis of multiple interactions between identical gene products because they occur naturally in the static environment of an assembled particle. Furthermore, simple viruses are accessible experimental systems for the study of mechanistic details associated with assembly-dependent maturation events and environmentally controlled changes in subunit structure that mediate RNA translocation across membranes. Selected examples of these features and the role of macromolecular interactions in their control will be discussed in this brief overview.

The publication costs of this article were defrayed in part by page charge payment. This article must therefore be hereby marked "*advertisement*" in accordance with 18 U.S.C. §1734 solely to indicate this fact.

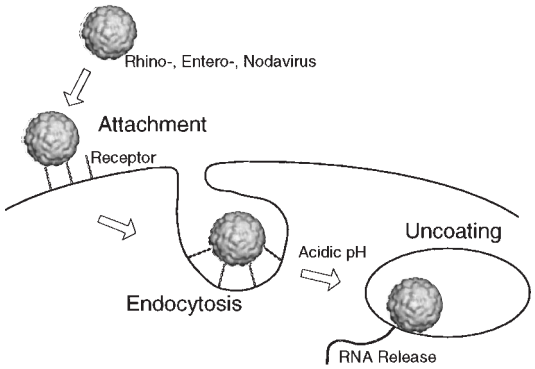


FIG. 1. Diagramatic representation of viral cell entry. The steps are based on experimental data from poliovirus and rhinovirus (2, 3) but similar steps are thought to occur for the nodaviruses.

The virus particle, which is composed of either a membrane enveloped or nonenveloped protein shell and nucleic acid, is designed to move its genome between cells of a susceptible host and between hosts. The viral gene products may be encoded on positive, negative, or double-stranded RNA or single- or double-stranded DNA. The protein shell provides a protective coat for the nucleic acid, carries out required chemical reactions for particle maturation, and facilitates entry into the cell (Fig. 1). Virus particles are always formed of multiple copies of identical gene products to minimize the genetic information required for shell formation. The simplest viruses are formed with 60 identical subunits and they are arranged with the symmetry of the icosahedron (532 point group symmetry, Fig. 2). Assembly of such a particle is straightforward to envision because all subunits are in identical structural environments. Once the proper complementarity of surfaces has evolved, formation of the symmetric particle is a logical consequence.

## Quasiequivalence

Icosahedral particles are common because they form the largest envelope in which all subunits are in identical environments. Subunits of simple viruses generally are composed of 200–400 amino acids and the shell formed by 60 subunits of this size is inadequate to package a genome encoding a full complement of proteins required for infectivity. The formation of larger shells, with a volume adequate to package an infectious genome, consists of integral multiples of 60 subunits with nonidentical quasiequivalent contacts between subunits. The geometrical basis for these particles was developed by Caspar and Klug (4) and it is established on the principle that the same subunits can form either hexamers or pentamers (5). Hexamers and pentamers are collectively referred to as morphological units in this review and they are considered as the formal building blocks of the quasiequivalent particle, rather than the individual subunits (Fig. 3). All quasiequivalent structures require molecular switches to control the formation of hexamers or pentamers and to determine the location of the different morphological units in the surface lattice.

In the sections below, the details of molecular switching and its effect on protein–protein interactions are discussed for various quasiequivalent surface lattices. Two positive-strand RNA viruses (≈300 Å in diameter) with $T = 3$ surface lattices dictated by different switching mechanisms are described. The first lattice type is represented by cowpea chlorotic mottle

Abbreviations: HRV, human rhinovirus; FHV, flock house virus.

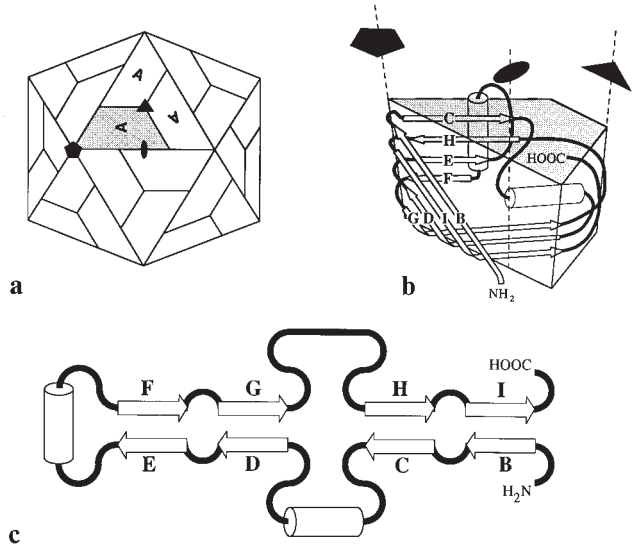


FIG. 2. Diagrammatic representation of an icosahedral virus particle and a generic diagram of the β-sandwich fold of the subunits observed in many RNA and DNA viruses. (*a*) The icosahedral capsid contains 60 identical copies of the protein subunit labeled A. These are related by fivefold (vertices), threefold (faces), and twofold (edges) symmetry elements. For a given sized subunit, this point group symmetry generates the largest possible assembly in which every protein lies in an identical environment. (*b*) A schematic representation of the subunit building block found in many RNA and some DNA virus structures. Such subunits have complimentary interfacial surfaces that, when repeated, lead to the symmetry of the icosahedron. The tertiary structure of the subunit is an eight-stranded β-sandwich with the topology of the jelly roll. Subunit sizes generally range between 20 and 40 kDa with variation among different viruses occurring at the N and C termini and in the size of insertions between strands of the β-sheet. (*c*) The topology of the viral subunit β-sandwich shown in *b*.

virus, a member of the bromoviridae and among the most intensely studied plant viruses. It was the first icosahedral virus assembled *in vitro* to form infectious virions and it has been the subject of biophysical studies for more than 25 years. A second $T = 3$ switching mechanism is found in nodaviruses, a family of bipartite RNA viruses infecting insects, mammals, and fish. Although less common than $T = 3$ capsids, $T = 4$ virions are formed by the enveloped togaviridae (≈700 Å diameter) and the nonenveloped tetraviridae (≈400 Å diameter) both of which are positive-strand RNA viruses. Molecular switching required for one form of this capsid type is described for Nudaurelia capensis ω virus, a tetravirus. A final example of polymorphic quaternary structures and their determinants is provided by the double-stranded circular DNA papovaviruses (≈500 Å in diameter), which display a pseudo $T = 7$ lattice containing only pentamers.

## $T = 3$ Particles

A particle with $T = 3$ quasisymmetry contains three chemically identical gene products in the icosahedral asymmetric unit. There are a number of examples of high-resolution structures of particles with this symmetry (6) and they form two distinct geometrical shapes. Cowpea chlorotic mottle virus is an example of the truncated icosahedron (Fig. 3*d*), while nodavirus particles have the geometry of the rhombic triacontahedron (Fig. 4). The truncated icosahedron most closely approximates the initial proposal put forth in the quasiequivalence theory (4). Subunits form particles with fivefold symmetry, required by the icosahedral point group, and nearly exact sixfold quasisymmetry. The sixfold axes are coincident with the threefold symmetry axes of the point group (Fig. 3 *b* and *d*). In contrast the rhombic triacontahedron does not form a true hexamer but, rather, a trimer of dimers about each of the icosahedral threefold axes (Fig. 4).

Formation of the hexamers in the cowpea chlorotic mottle virus-truncated icosahedra results from interactions in a region near the N termini of the subunits that form a β-structure about the icosahedral threefold axes (7). Residues forming the β-structure in the hexamers are disordered at the pentamer axes. The larger number of interactions at the hexamer suggests that this is the more stable of the morphological units and that pentamers form to increase the total number of interactions found in the closed icosahedral shell when curvature is induced by RNA and metal ions that are critical for the formation of particles at physiological pH (7). Reassembly products formed *in vitro*, without RNA or metal ions, are primarily tubes and sheets formed of only hexamers (8).

The rhombic triacontahedron structure observed in nodaviruses, tomato bushy stunt virus, and southern bean mosaic virus results from two distinctly different interactions between identical subunit interfaces. The particle observed in $T = 3$ nodaviruses is illustrated in Fig. 4. This polyhedral shape results from a molecular switch that differs in its configuration at the icosahedral and quasi-twofold symmetry axes. The switch is composed of a segment of an RNA duplex and/or a segment of polypeptide that has an ordered structure only at the icosahedral twofold symmetry interface (9–11). The switch functions as a wedge that prevents the pivoting of the protein surfaces in contact and this results in a nearly planar rhombic face. As the switch is not ordered at the quasi-twofold contact, the protein surfaces pivot about a line of residue interactions (conserved at both interface types) and this results in a dihedral angle of roughly 140° at this interface. It is the blend of these geometrically distinct joints that leads to a particle with 180 subunits. If all the contacts were flat, the protein would form sheets, and if all the contacts were bent, a 60-subunit $T = 1$ particle would result.

## $T = 4$ Particles

Recently, the structure of Nudaurelia capensis ω virus, a virus particle with $T = 4$ quasisymmetry, was solved at near atomic resolution. The differences in subunit contacts that determine its architecture are remarkably similar to those observed in the $T = 3$ rhombic triacontahedron (12). Switching occurs at two quasi-twofold contacts where one is flat and the other is bent. The switch in these structures is a segment of protein with an extended polypeptide in one portion and a five-turn helix in another. An additional alteration of subunit interactions occurs at the icosahedral threefold and the quasi-threefold axes, where internal helical interactions near the visible N termini of the subunits are slightly different in the two trimers.

## $T = 7$ Particles

Structures of simian virus 40 (13) and polyoma virus particles have $T = 7$ symmetry that illustrate a remarkable level of nonequivalence in virion assembly. The quasiequivalent surface lattice predicts a defined valency about each morphological unit. Pentamers have five neighboring morphological units and hexamers have six (Fig. 3*g*). The $T = 7$ surface lattice in observed structures (13) displays hexavalent and pentavalent morphological units as predicted, but hexavalent lattice points are occupied by pentameric morphological units (Fig. 5)! Contacts between morphological units are defined by either local or icosahedral twofold axes that the geo-

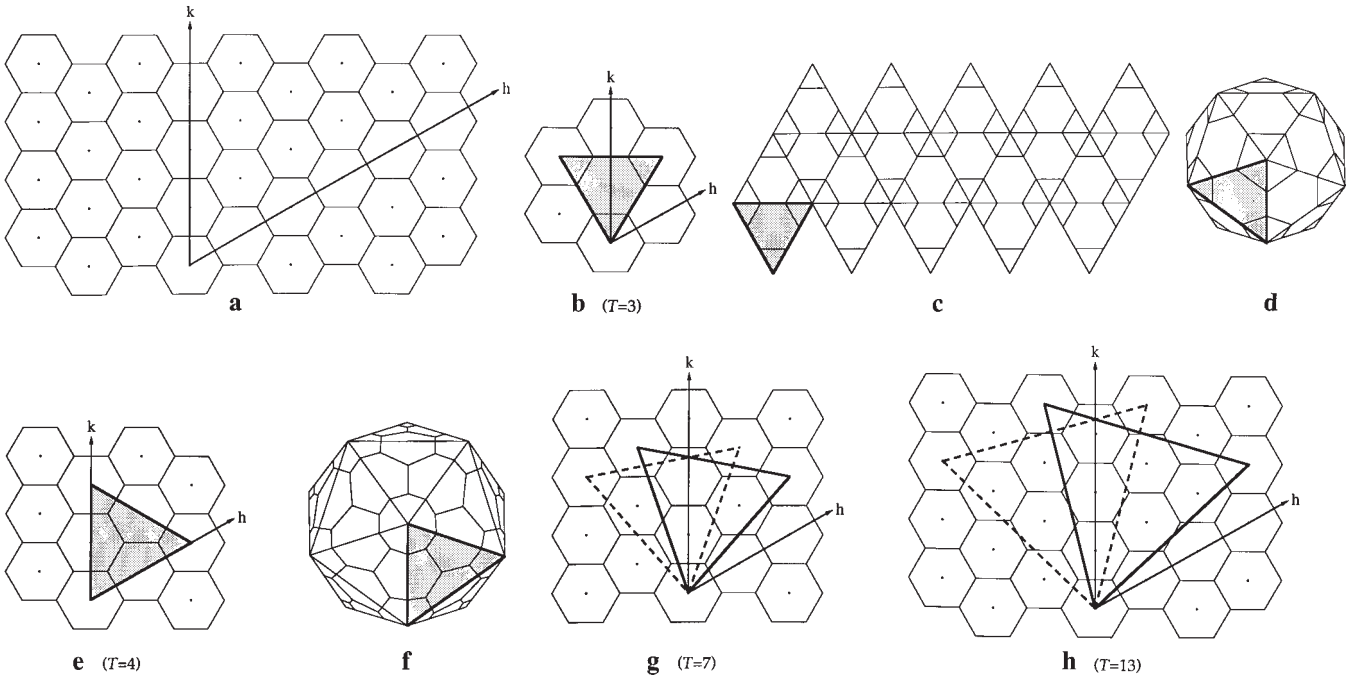


FIG. 3. Geometric principle for generating icosahedral quasiequivalent surface lattices and four examples of its application are illustrated. These constructions show the relation between icosahedral symmetry axes and quasiequivalent symmetry axes. The latter are symmetry elements that hold only in a local environment. (*a*) It is assumed in quasiequivalence theory that hexamers and pentamers can be interchanged at a particular position in the surface lattice. Hexamers are initially considered planar (an array of hexamers forms a flat sheet as shown) and pentamers are convex, introducing curvature in the sheet of hexamers where they are inserted. The closed icosahedral shell composed of hexamers and pentamers is generated by inserting 12 pentamers at appropriate positions in the hexamer net. The positions at which hexamers are replaced by pentamers are identified by the indices **h** and **k** along the labeled axes in the drawing. Once an origin is defined, every hexamer in the lattice can be uniquely identified by the number of steps along each axial direction required to reach that lattice point (**hk**). To construct a model of a particular quasiequivalent lattice, one face of an icosahedron is generated in the hexagonal net. The origin is replaced with a pentamer and the (**hk**) hexamer is replaced by a pentamer. The third replaced hexamer is identified by threefold symmetry (i.e., complete the equilateral triangle of the face). Each quasiequivalent lattice is identified by a number $T = \mathbf{h}^2 + \mathbf{hk} + \mathbf{k}^2$, where **h** and **k** are the indices described above. *T* indicates the number of quasiequivalent units in the icosahedral asymmetric unit. For the purpose of these constructions, it is convenient to choose the icosahedral asymmetric unit as one-third of an icosahedral face defined by the triangle connecting a threefold axis to two adjacent fivefold axes. Other asymmetric units can be chosen such as the triangle connecting two adjacent threefold axes and an adjacent fivefold axis (Fig. 4). The total number of units in the particle is $60T$, given the symmetry of the icosahedron. The number of pentamers must be 12 and the number of hexamers is $(60T - 60)/6 = 10(T - 1)$. (*b*) One face of the icosahedron for a $T = 3$ surface lattice is identified. The hexamer replaced has coordinates $\mathbf{h} = 1$ and $\mathbf{k} = 1$. The icosahedral asymmetric unit is one-third of this face and it contains three quasiequivalent units (two units from the hexamer coincident with the threefold axis and one unit from the pentamer). (*c*) The three-dimensional model of the quasiequivalent lattice can be generated by arranging 20 identical faces of the icosahedron as shown. (*d*) The folded icosahedron is shown with hexamers and pentamers outlined. The shaded face represents the triangle originally generated from the hexagonal net. The $T = 3$ surface polyhedron represented in this construction is a truncated icosahedron and it has the appearance of a soccer ball. (*e*) An example of a $T = 4$ icosahedral face ($\mathbf{h} = 2$ and $\mathbf{k} = 0$). In this case the hexamers are coincident with icosahedral twofold axes. (*f*) A folded $T = 4$ icosahedron with the shaded face corresponding to the face outlined in the hexagonal net. Note that folding the lattice has required that the hexamers have the curvature of the icosahedral edges. (*g*) A single icosahedral face generated from the hexagonal net for a $T = 7$ lattice. Note that there are two different $T = 7$ lattices ($\mathbf{h} = 2$ and $\mathbf{k} = 1$; heavy outline and $\mathbf{h} = 1$ and $\mathbf{k} = 2$; dashed outline). These lattices are the mirror images of each other. To fully define such a lattice the arrangement of hexamers and pentamers must be established as well as the enantiomorph of the lattice. (*h*) A single icosahedral face for a $T = 13$ lattice is shown. The two enantiomorphs of this quasiequivalent lattice ($\mathbf{h} = 3$ and $\mathbf{k} = 1$, solid; $\mathbf{h} = 1$ and $\mathbf{k} = 3$, dashed) are outlined. Note that the procedure for generating quasiequivalent models described here does not exactly correspond to the one described by Caspar and Klug (4). Caspar and Klug (4) distinguish between different icosadeltahedra by a number $P = \mathbf{h}^2 + \mathbf{hk} + \mathbf{k}^2$, where **h** and **k** are integers that contain no common factors but 1. The deltahedra are triangulated to different degrees described by an integer *f*, which can take on any value. In their definition, $T = Pf^2$. The description in this figure has no restrictions on common factors between **h** and **k**; thus, $T = \mathbf{h}^2 + \mathbf{hk} + \mathbf{k}^2$ for all positive integers. The final models are identical to those described by Caspar and Klug (4).

metric theory predicts to be closely similar. Because all morphological units are pentamers in the $T = 7$ structures observed, interactions within morphological units are virtually identical but quasi- and icosahedral twofold axes relating morphological units are grossly different. The changes in contacts between morphological units required to accommodate this lack of quasiequivalence are all mediated by order–disorder alterations in the C-terminal portion of the subunit polypeptide (13).

## Virus Maturation After Assembly

The virus particle is not an inert device for transporting nucleic acid. It plays an active role in the processes illustrated in Fig. 1. To accomplish these ends many virus particles undergo maturation events after assembly that are required for infectivity. The picornaviruses (14) and the nodaviruses (15) have been analyzed in the context of available high-resolution structures. In both cases the processing is autocatalytic and is dependent upon proper particle assembly. Picornaviruses are a major causative agent of disease in humans and other animals. They are icosahedral viruses (≈300 Å in diameter) with a positive-strand RNA genome. Their structures are similar to $T = 3$ particles (Fig. 4), except the capsid contains three primary gene products instead of one. It is likely that the gene for a single subunit in a $T = 3$ virus triplicated and that this allowed the independent evolution of the three subunits in the icosahedral asymmetric unit. Capsid gene products desig-

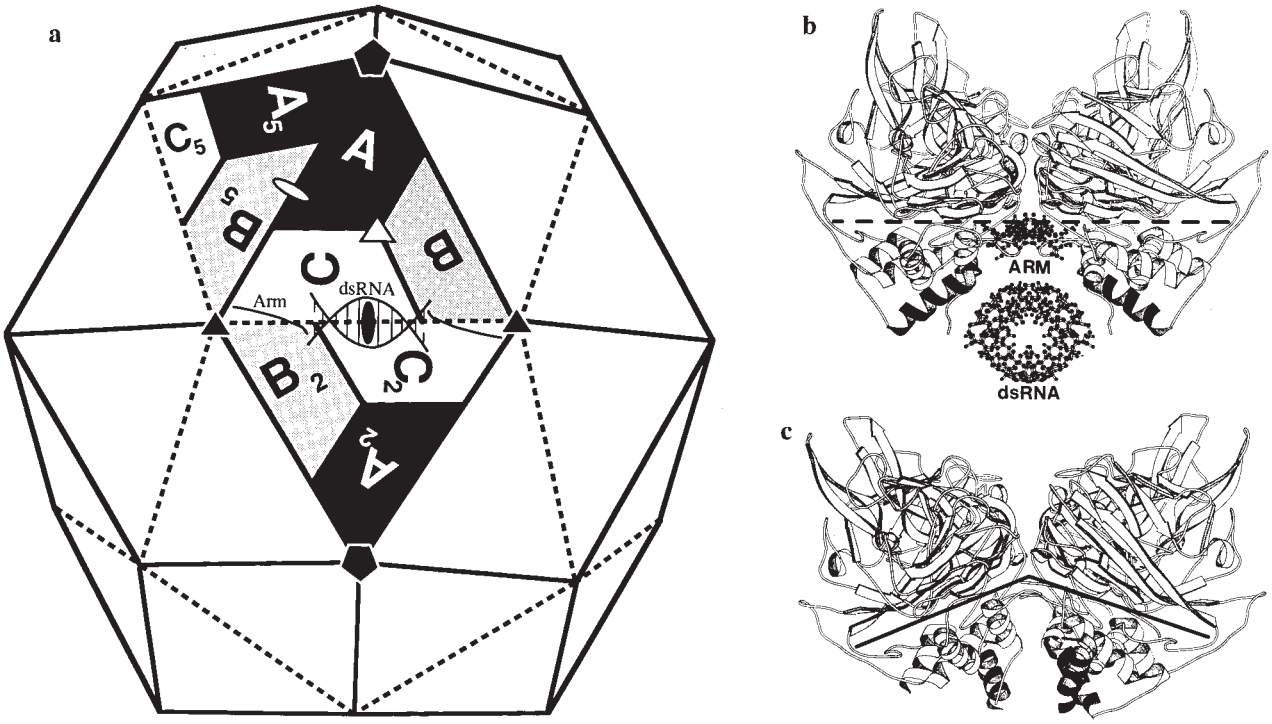


FIG. 4. Capsid protein subunit interactions as seen in the structure of flock house virus (FHV), a nodavirus. (*a*) A schematic drawing of the entire capsid of the $T = 3$ FHV with the subunits labeled for three icosahedral asymmetric units. The molecular switch required for $T = 3$ particle formation in this virus is a peptide (residues 20–31) from the C subunit and segments of duplex RNA that are ordered only at the icosahedral twofold axes as illustrated (the icosahedral twofold, threefold, and fivefold are represented by the solid oval, triangle, and pentagon, respectively, and the quasi-twofold and threefold are represented by the open oval and triangle). (*b*) A tangential view of the four subunits (C, $C_2$, B, and $B_2$) at the icosahedral twofold axis (vertical in the plane of the page). This contact is flat because the peptides and duplex RNA bind under the subunits and act as a wedge. The peptides are drawn as ball-and-stick above the duplex RNA helix also drawn as ball-and-stick. The cleavage products ($\gamma$) are drawn as solid $\alpha$-helices. (*c*) The RNA and peptide do not bind under the four subunits (A, $B_5$, C, and $A_5$) at the quasi-twofold (vertical in the plane of the page) allowing the subunits to form a bent contact. $\gamma$ peptides are drawn as solid $\alpha$-helices ($\gamma$ is not seen in the B subunit). dsRNA, double-stranded RNA.

nated VP1, VP2, and VP3 are each eight-stranded $\beta$-sandwich structures (Fig. 2) and they occupy positions analogous to the A, C, and B, respectively, in the $T = 3$ capsid. A fourth gene product, VP4, is internal and assembles initially as the N-terminal extension of VP2. Each pseudo-equivalent interface (interfaces that are quasiequivalent in $T = 3$ particles) has evolved to form complimentary interactions through the unique sequences of VP1, VP2, and VP3, precluding the need for a switch. Picornavirus messenger-sense RNA genomes are translated as a polyprotein that is subsequently processed by virally encoded proteases. The picornavirus capsid is initially assembled as 60 copies of VP0, VP3, and VP1 (corresponding to the gene order from the 5′ end of the RNA) and an RNA molecule. VP0 contains VP2 and VP4.

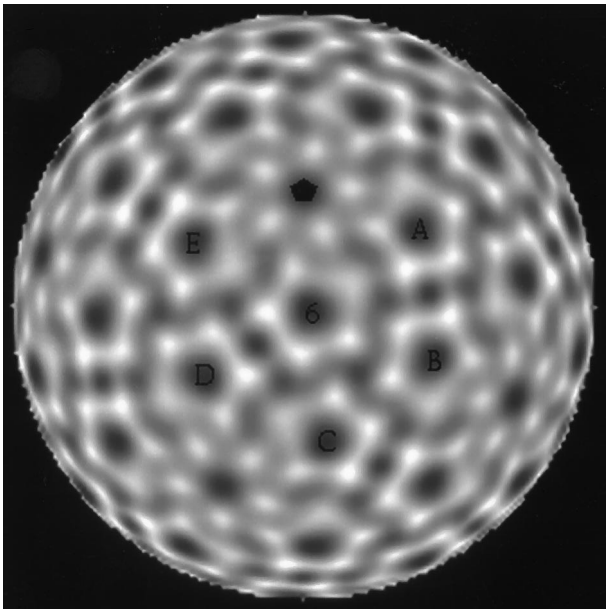


FIG. 5. Structure of bovine papilloma virus determined by image reconstruction of cryoelectron micrographs. The density displayed is at a radius of 230 Å. The pentamers are situated on a classical $T = 7$ surface lattice with pentavalent (indicated by a solid pentagon) and hexavalent (labeled with a 6 and with letters) lattice positions but all are occupied by pentamers.

The final processing of picornaviruses occurs after assembly and near the N terminus of the precursor protein VP0 to release VP4 and VP2. VP4 is a 68-residue myristoylated polypeptide in poliovirus and human rhinovirus (HRV) 14 that is internal to the capsid protein. VP4 is implicated in early events of cellular entry (see below) and it is lost from the particle after binding to the receptor (e.g., ref. 2). The mechanism of the cleavage has not been established, but the site is not accessible to the surface and the processing probably involves the packaged RNA as a nucleophile (14).

Nodavirus processing generates an infectious particle by cleaving the full-length subunit $\alpha$ (residues 1–407) at residue 363 to generate $\beta$ (residues 1–363) and $\gamma$ (res-

idues 364–407) chains. The γ chains are amphipathic helices that interact with RNA about the icosahedral threefold axes (B and C subunits in Fig. 4) and form a helical bundle at the fivefold axes (A subunits in Fig. 4). The disposition of the cleaved polypeptides within the capsid is shown in Fig. 6. A structure-based mechanism for this cleavage, supported by site-directed mutations, has recently been reported (16). Assembly stabilizes the position of Asp-75 that is buried in a hydrophobic environment resulting in an abnormally high $pK_a$ of 6.8. Asp-75 is protonated under physiological conditions and serves as a proton donor for a hydrogen bond to the carbonyl oxygen of Asn-363. Assembly locally destabilizes the scissile bond between residues 363 and 364 making it susceptible to attack by a water molecule (possibly activated by the anionic environment of the directly adjacent bulk RNA). The mature particle is more stable than the uncleaved provirion due to the release of stress at the active site when cleavage occurs. The kinetics of the cleavage are consistent with a reaction that slows down at a rate that is proportional to the number of cleavages that occur. Generally 10–20% of the subunits remain uncleaved after an extended period of time because the overall stability of the particle no longer drives the reaction. The observed behavior is consistent with the distribution of stress in geodesic domes known as tensegrity (17). The half-life for 80% of the subunits to cleave is ≈4 hr. The cleavage site, the proposed mechanism, and a cartoon of the energetics suggested by the kinetics of the reaction are shown in Fig. 7. It has recently been noted that a nearly identical mechanism for cleavage exists in the $T = 4$ tetraviruses (12).

### Events in Cell Binding and RNA Release

Initial interactions between a virus and a susceptible cell can occur through a variety of surface molecules present on the cell. Recently, there have been a number of virus receptors identified (tabulated in ref. 3). The interaction of the rhinovirus major group receptor, intercellular adhesion molecule 1 (ICAM1), and HRV16 has been visualized with cryoelectron microscopy, and details of the interaction have been developed on the basis of an ICAM model and the high-resolution x-ray structure of HRV16 (18). Receptor binding to poliovirus is likely to occur in a manner very similar to that observed in HRV16. A different mode of interaction with a receptor is anticipated for foot and mouth disease virus where a highly exposed RGD sequence located on a flexible loop interacts with a cell surface molecule as the first step in cell entry.

Effects of binding to the cellular receptor have been well characterized for po-

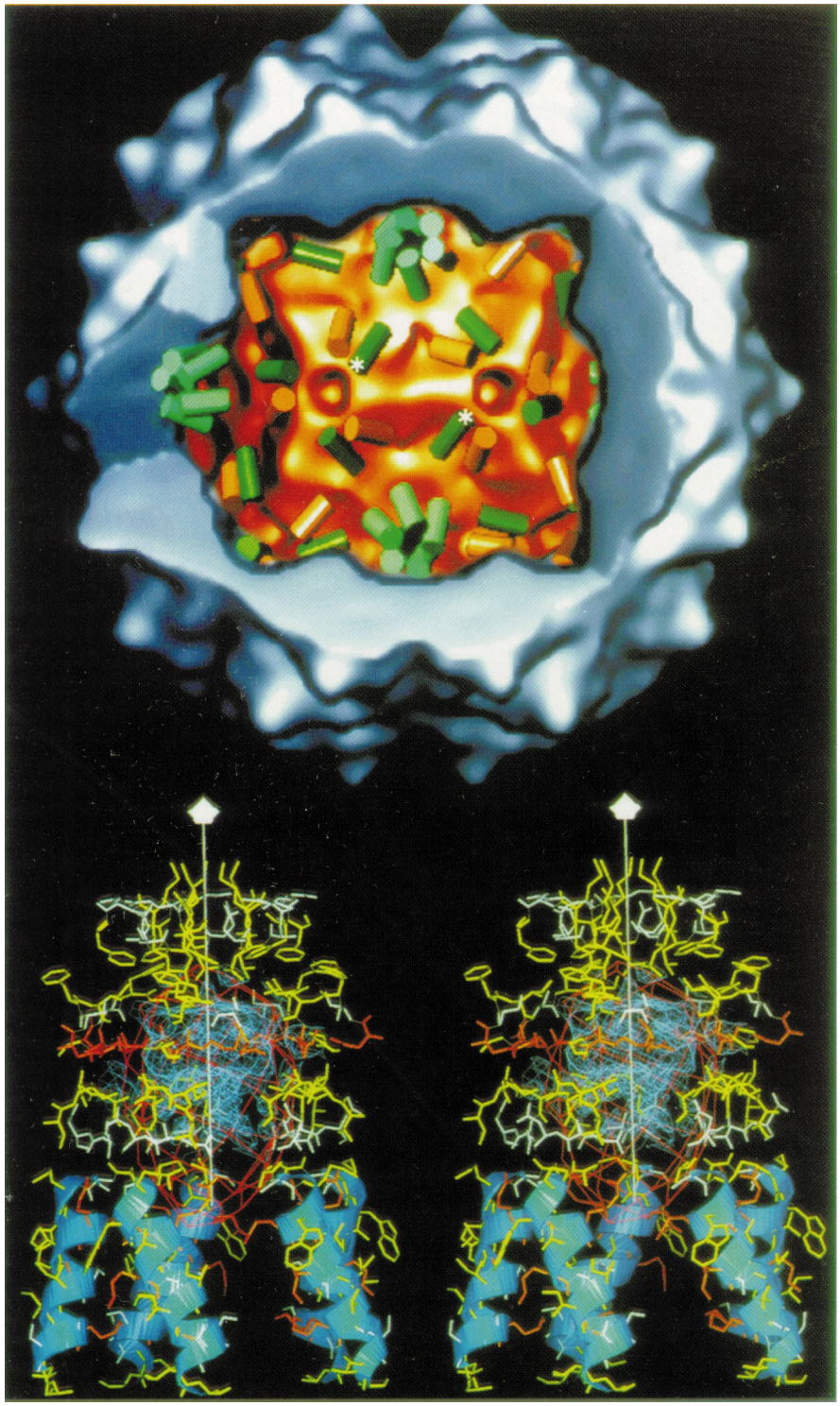

FIG. 6. (*Upper*) Global cut-away view of FHV including the electron density for the protein shell derived from the cryoelectron micrograph reconstruction (blue), the RNA density derived from a difference electron density map (red), and the disposition of the cleaved γ-peptide helices, which are based on the x-ray coordinates, represented as cylinders. The $\gamma_B$ (red) and $\gamma_C$ (green) helices associated with the B and C subunits interact with bulk and ordered RNA and are clustered about the icosahedral threefold axes. The $\gamma_A$ helices (blue) are clustered about the fivefold symmetry axes and do not contact the RNA except at their C termini, where residues 383–407 display no density and appear to be associated with the RNA. The cleavage site (see Fig. 7*a* for a close view) in all the helices (Asn-363 and Ala-364) is at the end that lies at higher radius and closest to the symmetry axis. (*Lower*) A close view of the $\gamma_A$ helices which form helical bundles about each of the fivefold symmetry axes of the particle. The fivefold axis is vertical. The cleavage site is at the top of the strongly amphipathic helices. Only a portion of the A subunit model is shown. All of the residues that are close to the fivefold symmetry axes are hydrophobic, forming a potential channel for the escape of the cleaved γ-polypeptide bundle, which has a hydrophobic surface and a hydrophilic core.

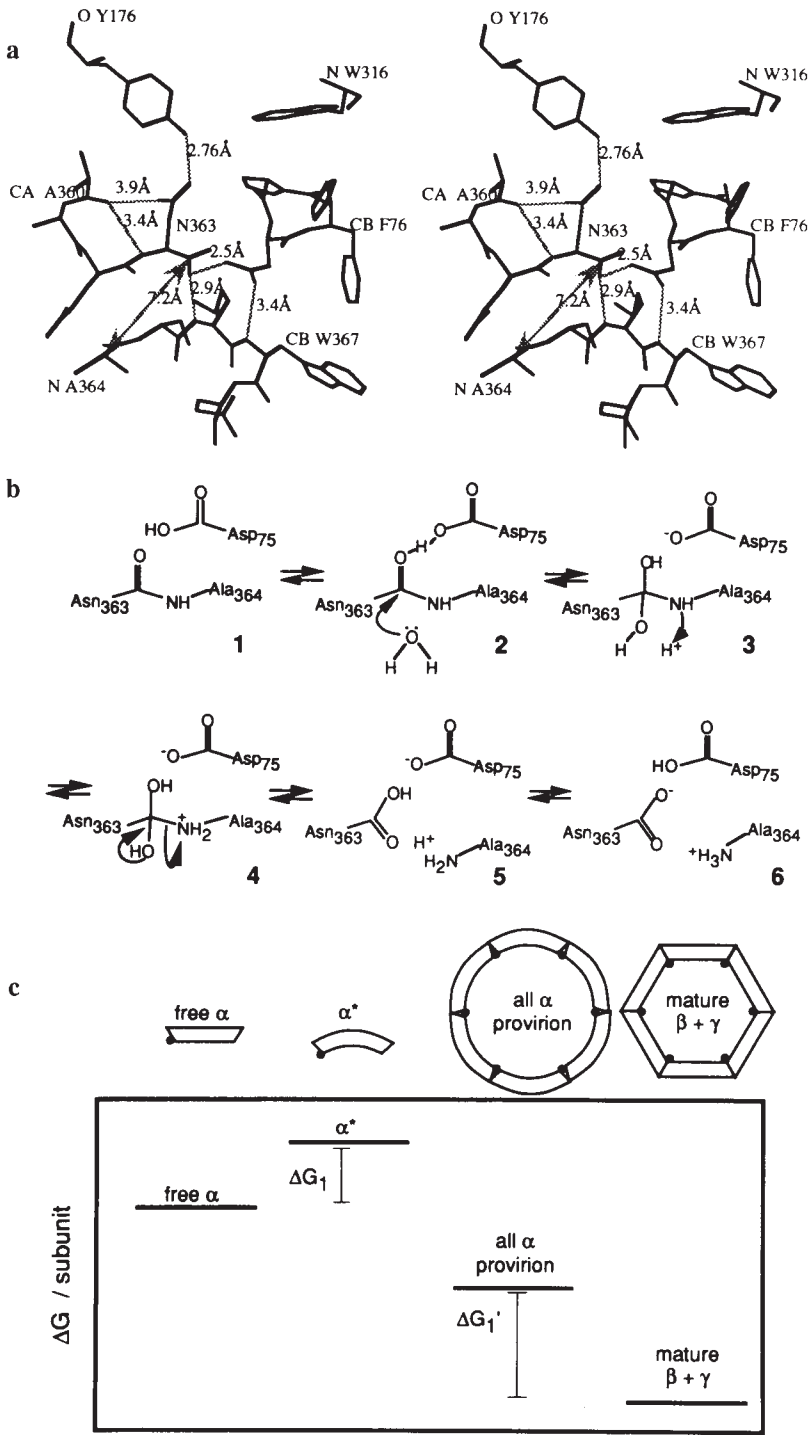


FIG. 7. (*a*) Structure of the solvent-occluded cleavage site of FHV. The network of hydrogen bonds directs interactions among Asn-363, the C terminus of the $\beta$ protein, and Asp-75. Functional groups that participate in hydrogen bonding interactions are conserved within the nodavirus family. Asn-363 is the last residue in a type 1 $\beta$-turn where both the side chain and peptide amides donate hydrogens to the carbonyl of Ala-360. The side-chain carbonyl of Asn-363 accepts a hydrogen bond from the phenolic hydroxyl of Tyr-176. Tyr-176 is on the D strand of the coat protein subunit's $\beta$-barrel. These interactions direct the C terminus of Asn-363, created by proteolysis, toward the side-chain carboxylic acid of Asp-75, forcing protonation of one or both of the two acids at physiological pH and formation of a hydrogen bond. The C-terminal carboxyl also accepts a hydrogen bond from the peptide amide of Ser-365 in the $\gamma$ peptide. Asp-75 accepts a hydrogen bond from the peptide amide of Met-366. (*b*) The proposed mechanism for the autoproteolytic maturation of the nodavirus capsid protein results from chemical (Fig. 7*a*) and thermodynamic (Fig. 7*c*) factors affected by assembly. Asp-75 is highly protonated even at neutral pH by virtue of its burial in a hydrophobic environment stabilized by the association of subunits during assembly (**1**). It forms a hydrogen bond with the carbonyl of the peptide bond between Asn-363 and Ala-364 and this is sufficient to make it susceptible to nucleophilic attack by water (**2**) to form a tetrahedral intermediate (**3**). The water molecule is not trapped within the cleavage site but probably originates from within the hydrophilic interior of the virus capsid. The intermediate can relax by loss of the amine from the nascent peptide (**4** and **5**), yielding the hydrolyzed peptide bond at the cost of one water molecule (**6**). The hydrophobic protonation/activation of a catalytic acid residue resembles the activation of the catalytic Asp in lysozyme. Conversely, in the typical acid protease, it is the close interaction between two Asp residues that is responsible for the elevated $pK_a$ of one of the catalytic acids. (*c*) A scheme describing the thermodynamics of virus assembly and maturation. The cartoon relates the activation and relaxation of the coat protein subunits in the course of capsid assembly and maturation. The free energy of activated $\alpha^*$, $\alpha$ protein in the provirion but not including the stabilizing free energy from quaternary interactions, is greater than that of free $\alpha$ protein by $\Delta G_1$, and this energy may stabilize an intermediate in the cleavage. Quaternary interactions stabilize formation of the relatively unstable provirion favoring spontaneous assembly. Autoproteolytic maturation is energetically driven by $\Delta G_1$, the combination of energy gained by relaxation of the strained provirion conformation of the coat protein and the change in free energy of intersubunit interactions in the mature capsid. Although the provirion and mature particle are drawn as substantially different structures, the two particles are nearly identical in their physical parameters (sedimentation coefficient and diameter). The gain in particle stability is accompanied by a very subtle change in quaternary structure.

liovirus (2) and HRV (3). In both cases, there are substantial conformational changes to the particles that decrease their sedimentation coefficients and increase their ability to bind liposomes. Binding the receptor causes poliovirus to turn the N-terminal portion of VP1 inside out with the proposed formation of an amphipathic helix that allows particle binding to liposomes. The particle alteration and interaction with the membrane has been compared with the first events of membrane fusion in enveloped viruses, with interactions at the membrane assisting the translocation of RNA.

Although little experimental work has been performed for nodaviruses, the high-resolution structures and preliminary analyses by electron microscopy suggest that events associated with cell attachment and RNA release may be similar to poliovirus and HRV, although different in detail (19). The nodavirus structures all contain pentameric helical bundles at the fivefold axes (Fig. 6) and the helices are composed of the cleaved $\gamma$ peptides. The ordered region extends from residues 364 (the first residue of the cleaved polypeptide) to 384 (where the helix stops at a Pro-Gly-Pro sequence that is conserved in nodaviruses). Residues 385–407 (the C terminus) are not visible in the electron density. The helices are amphipathic with hydrophilic residues inside the bundle and hydrophobic residues in contact with the internal surface of the subunits. The organization of the helical bundle is similar to that proposed for channel formation in other channel forming systems (20), and

the length of the helices is sufficient to span the lipid portion of the membrane bilayer.

A model currently being tested for nodaviruses is based on the release of the pentameric bundle induced by interactions among the virus, its receptor, and the endosomic membrane, with the helical bundle forming a hydrophilic pore for the RNA to translocate across the membrane. The driving force for RNA translocation may come from translation of the RNA into protein if the ribosome binding site is exposed to the cytosol. The concept of cotranslational disassembly for RNA plant viruses is now an established mechanism for infection (21) and it may be important for the RNA animal viruses as well.

## Conclusions

The examples discussed illustrate that, within the context of their primary role of packaging and moving nucleic acid, viral subunit proteins perform a variety of biological functions. Each virus examined displays a switch for altering subunit interfaces required for the synthesis of quasiequivalent capsids. Subunit interactions control the timing of maturation processing in the animal viruses examined and the resulting cleavages allow the release of prefabricated modules, presumably to translocate RNA across membranes.

Prof. Tom Smith is gratefully acknowledged for preparing Fig. 1. Sanjeev Munshi, Vijay Reddy, Adam Zlotnick, and Tom Smith provided stimulating discussions and suggestions. Fig. 5 was provided by David Belnap and Tim Baker.

1. Milligan, R. (1996) *Proc. Natl. Acad. Sci. USA* **93,** 21–26.
2. Fricks, C. E. & Hogle, J. M. (1990) *J. Virol.* **64,** 1934–1945.
3. Rossmann, M. G. (1994) *Protein Sci.* **3,** 1712–1725.
4. Caspar, D. L. D. & Klug, A. (1962) *Cold Spring Harbor Symp. Quant. Biol.* **27,** 1–24.
5. Johnson, J. E. & Fisher, A. J. (1994) *Encyclopedia of Virology* (Academic, New York), pp. 1573–1586.
6. Rossmann, M. G. & Johnson, J. E. (1989) *Annu. Rev. Biochem.* **58,** 533–573.
7. Speir, J. A., Munshi, S., Wang, G., Baker, T. S. & Johnson, J. E. (1995) *Structure* **3,** 63–78.
8. Bancroft, J. B. (1970) *Adv. Virus Res.* **16,** 99–134.
9. Olson, A. J., Bricogne, G. & Harrison, S. C. (1983) *J. Mol. Biol.* **171,** 61–93.
10. Abad-Zapatero, C., Abdel-Meguid, S. S., Johnson, J. E., Leslie, A. G. W., Rayment, I., Rossmann, M. G., Suck, D. & Tsukihara, T. (1980) *Nature (London)* **286,** 33–39.
11. Fisher, A. J. & Johnson, J. E. (1993) *Nature (London)* **361,** 176–179.
12. Johnson, J., Munshi, S., Liljas, L., Agrawal, D., Olson, N., Reddy, V., Fisher, A., McKinney, B., Schmidt, T. & Baker, T. (1994) *Arch. Virol.* **9,** 497–512.
13. Liddington, R. C., Yan, Y., Moulai, J., Sahli, R., Benjamin, T. L. & Harrison, S. C. (1991) *Nature (London)* **354,** 278–284.
14. Rossmann, M. G., Arnold, E., Erickson, J. W., Frankenberger, E. A., Griffith, J. P., Hecht, H. J., Johnson, J. E., Kamer, G., Luo, M., Mosser, A. G., Rueckert, R. R., Sherry, B. & Vriend, G. (1985) *Nature (London)* **317,** 145–153.
15. Gallagher, T. M. & Rueckert, R. R. (1988) *J. Virol.* **62,** 3399–3406.
16. Zlotnick, A., Reddy, V. S., Dasgupta, R., Schneemann, A., Ray, W. J., Rueckert, R. R. & Johnson, J. E. (1994) *J. Biol. Chem.* **269,** 13680–13684.
17. Fuller, R. B. (1975) *Synergistics* (Macmillan, New York).
18. Olson, N., Kolatkar, P., Oliveira, M., Cheng, R., Greve, J., McClleand, A., Baker, T. & Rossmann, M. (1993) *Proc. Natl. Acad. Sci. USA* **90,** 507–511.
19. Cheng, R. H., Reddy, V. S., Olson, N. H., Fisher, A. J., Baker, T. S. & Johnson, J. E. (1994) *Structure* **2,** 271–282.
20. Parker, M. W. & Pattus, F. (1993) *Trends Biochem. Sci.* **18,** 391–394.
21. Roenhorst, J. W., Verduin, B. J. M. & Goldbach, R. (1989) *Virology* **168,** 138–146.